Chapter 4: Study of Incremental Sheet Forming for Complex Shape and its Improvement

4.1 Introduction

Incremental sheet forming (ISF) is an innovative process to manufacture sheet metal products by the (CNC) controlled movement of a simple forming tool which plastically deforms the blank according to the desired shape. The two main variations of incremental sheet forming are positive and negative forming. This refers to the side of the part that the tool works on. In negative forming the tool works on concave surface on the part, whereas in positive forming the tool moves on the convex surface. When the die has a positive geometry, the blank holder should be moved by hydraulic actuator in order to firmly maintain the sheet in proper working position; in the case of negative geometry, the blank can be fixed. Although it is a slow process, makes it a very suitable process for low series production, prototype manufacturing and complex components produced in small batches for aeronautical, automotive and medical applications due to the cost reduction linked to the fact that punches or dies are avoided, in comparison with the traditional stamping or drawing processes. This kind of process could go back to the conventional spinning process [55, 56] in which only axi-symmetric parts can be made. Besides, many other processes which can make both non-axi-symmetric parts as well as axi-symmetric parts have been developed. An incremental sheet forming process to make flanged sheet metal parts without dedicated tooling was developed by Powell *et al.* [57]. Matsubara [58] successfully formed various conic and pyramidal parts with the (NC) milling machine. Iseki and Kumon [59] have studied a forming limit for the incremental sheet forming process. They had shown that the forming limit curve (FLC) of sheet material in incremental sheet forming is located much higher than those based on theories of plastic instability. In order to investigate the influence of the main material parameters and process variables upon formability and improve the formability in incremental sheet forming several researches had been proposed [60, 61, 62**]**. Kim and Yang [63] proposed the double-forming technique to improve formability, assuming that only shear deformation occurs in the material. Recently, G. Hussain, and L. Gao *et al.* [64, 65, 66] presented an innovative method to test the thinning limits of sheet metals in negative incremental sheet forming along with verification of the

ISBN: 978-81-936820-9-8
Thesis DOI: 10.21467/books.75

Cosine's law of thickness distribution. They also showed that the formability in single point incremental sheet forming can be expressed as the maximum wall angle (θ_{max}). Besides, the effect of the curvature of a part's generatrix on the formability of an aluminum sheet has been investigated systematically to indicate that the formability increases as the radius of curvature decreases. Park *et al.* [67] studied and showed the possibility of cup incremental sheet forming of magnesium sheet at room temperature with rotational, where the tool rotates itself.

When manufacturing a complex shape by incremental forming, firstly a (CAD) file of the completed formed part must be designed, imported to (CAM) software, and simulated to generate the tool path or (CL) data file. Depending on the complexity of the part, the process can include a basic geometry supporting die or no dies at all. The tool path contours are then imported and performed on a standard (CNC) mill. For this kind of process in order to enhance the formability of sheet material in incremental sheet forming process, there are many process variables to be improved, such as the material properties, forming conditions, the shapes of the forming tool, curvature of part, dimension of forming part, specially down-step, offset tool path, and spindle speed also. These factors determine the formability, as regards the thickness variation, and blank failure after the incremental forming. As already pointed out in Ambrogio *et al.* [68] work, the single point incremental sheet forming process mainly depends on geometrical and process conditions. Particularly, the accuracy of the final geometry is mainly influenced by the tool down step.

Nowadays, numerical simulation is an essential tool for understanding of physical processes modelized by partial differential or integral Equations. After the pioneers work of finite-element method (FEM) for rigid-plastic FEM [69, 70, 71], elastic-plastic FEM [72, 73], (FEM) has been successfully applied to various kinds of sheet forming processes such as stamping [74, 75], hydroforming [75, 76], incremental sheet forming [68, 77, 78] etc., to clarify the forming characteristics, predict forming defect and improve the forming process. For incremental sheet forming the finite element analysis was also successfully used to study the effect of process variable on formability of materials in incremental sheet forming. In order to simulate incremental sheet forming by the finite element analysis, two different approaches could be pursued, namely an implicit model implementing a Lagrangian formulation or an explicit model. As shown by Ambrogio *et al.* [68] the use of explicit finite element simulation is a realistic and cost-effective method in predicting and investigating the effect of process variables on formability of incremental sheet metal forming. Several other studies were focused on the (FEM) analysis, taking into account simple shapes. Shim and Park [77] performed a numerical simulation of the single layer in the forming of truncated pyramid to find the deformation characteristics along the tool path. Iseki [78] simulated the incremental sheet forming of a shell of the frustum of a quadrangular pyramid. However, almost previous researches have focused on simple geometry models such as rectangular, circular geometries or the combination of both in simulation model.

In this study, the incremental sheet forming process for the product of complex geometry shape (e.g. human face) is studied using ABAQUS/Explicit finite element code and is improved using Taguchi's method. The input file was obtained by the combination of (CAM) and (CAE) simulation through using MATLAB programming. Figure 4.1(a) shows the tested sample in which failure occurred under improper forming conditions, the tool radius of 6 mm, the tool down-step of 2.0 mm, and the feed rate of 400 mm/min without rotating of the tool. The supported die is shown in Figure 4.1(b).

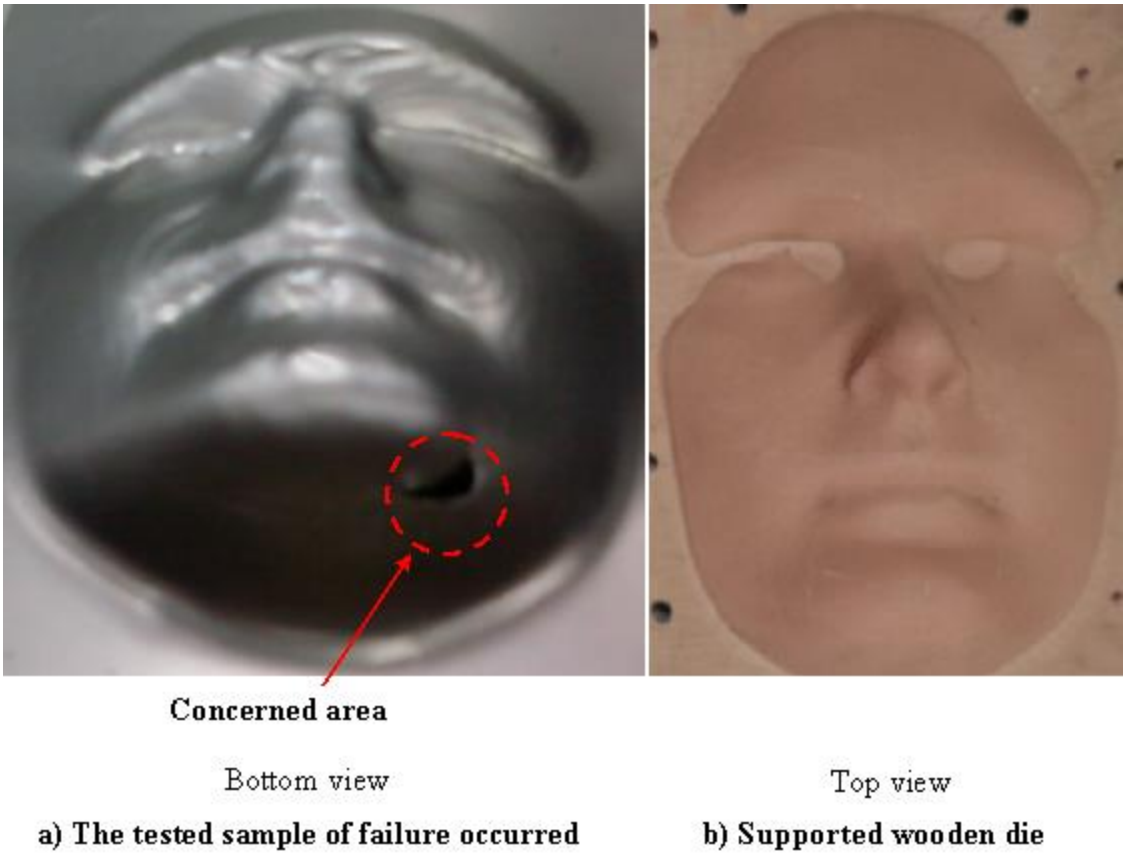

Figure 4.1: *Deformed shapes in experiment of failure test sample.*

Figure 4.2 depicts (FEM) simulation results for tested sample. The effects of forming variables, such as tool radius, tool down-step, friction coefficient, etc. are then investigated to determine their influence on the formability by comparing with forming limit curve. Taguchi's experimental technique is adopted to achieve the improved condition of these process variables.

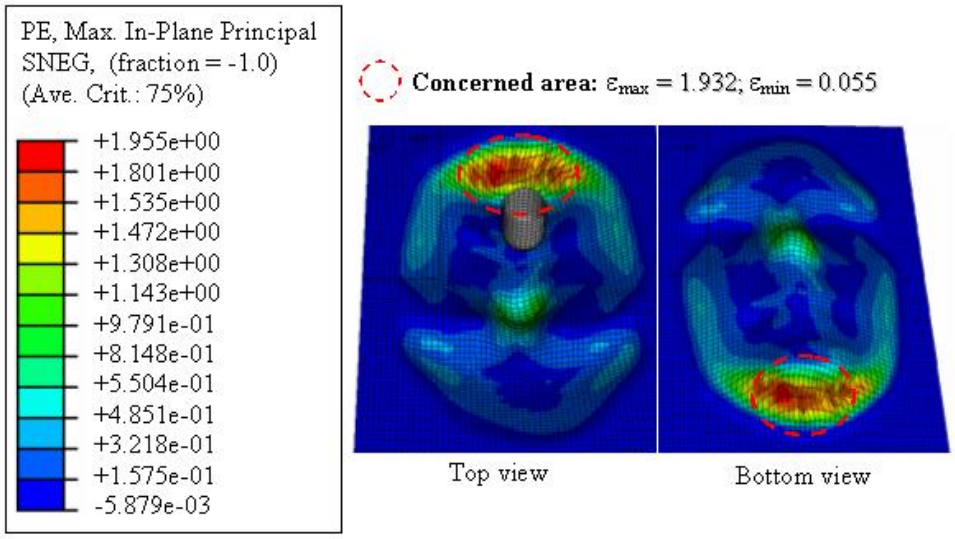

(a)

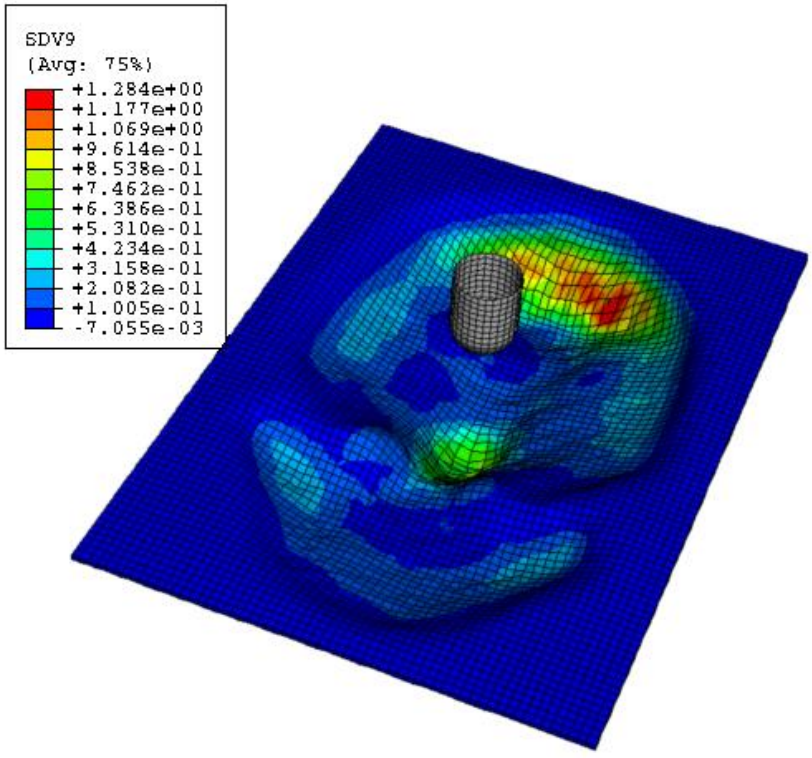

(b)

Figure 4.2: *The FE simulations for a failure test sample.*

4.2 Finite Element Simulation

This study used the commercial software ABAQUS version 6.5-1 to simulate the forming process. This software can provide elastic-plastic and rigid-plastic simulations of metal forming in the case of a large deformation, thereby significantly reducing the cost and time involved in tool and die design.

The flow pattern, equivalent stress distribution, equivalent strain distribution, and major and minor strains can all be simulated by (FEM). These simulation results can then be used to obtain the product geometric profile and material properties required. In the pre-process of modeling metal forming, the 3D mechanical type, geometric profile of the blank, and contact surfaces are constructed using the (GUI) of ABAQUS version 6.5-1. An elastic-plastic model is then selected and the material properties, such as Young's modulus, Poisson's ratio, and the density, are needed. The anisotropic work-hardening rule is applied in the flow rule due to plastic strain hardening. The changes in the Von-Mises stress, major and minor strains yielded on the surface are plotted. The initial conditions of the components are set-up, and the contact between the blank, punch, and die is defined.

4.2.1 Geometry and FE models

Figure 4.3 shows the finite-element model for the incremental sheet forming test process. Here, the tool and die model were made from the shape of the product using CATIA software, the blank modeled using both of shell elements S4R without VUMAT subroutine and solid elements C3D8R via VUMAT user material, and the punch and die modeled using rigid surface-elements R3D4. Throughout this study, the average element size of the blank and rigid tool was about 1 mm in width, and 1 mm in length; the average element size of the rigid die was about 2 mm in width, and 2 mm in length.

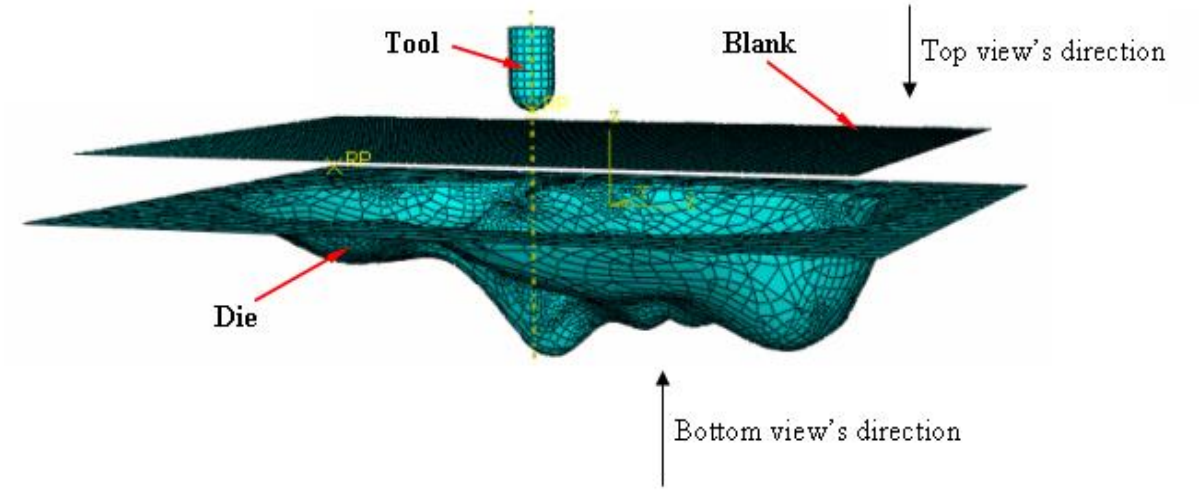

Figure 4.3 *Finite element model for simulation.*

4.2.2 Materials

Table 4.1 shows the mechanical properties of the blank, a cold rolled steel. The parameters characterizing the uniaxial-stress-plastic-strain response of the material used in the (FE) simulations are also given in the Table in terms of the parameters in Swift's work-hardening law, using the expression of Equation (3.1).

Table 4.1: *Mechanical properties of tested material (Cold Rolled Steel)*

Material	Cold Rolled Steel
Density (ρ)	7.8e-06
Young's modulus (E)	210
Possion's ratio	0.3
Tensile strength (MPa)	140
ε_0	0.0009
K (MPa)	534.1
n-value	0.274
Lankford value R_m	1.679

4.2.3 Boundary conditions, loading, and interactions

The die was fixed in all directions. The tool was allowed to move following the tool-path which was obtained from (CAM) simulation. The friction behavior was modeled using the Coulomb friction law. The friction coefficient μ_1 between the blank and the punch is assumed to be the same as the fiction coefficient μ_2 between the blank and the die.

4.2.4 Ductile fracture criterion

In order to predict the failure of the incremental forming for complex shape the criterion of Oyane is employed as Equation (3.2), Here, C_1, C_2 are simply determined by uniaxial and plane-strain tension tests [24]. The material constants C_1, and C_2 for the ductile fracture criterion were calculated as 0.15, and 0.76, respectively.

4.3 Obtained CAE input file procedures

4.3.1 Tool path generation

In order to obtain cutter location (CL) data for human surface, (3D) scanner is used to create a point cloud of geometric samples on the surface of the object. These points can be used to extrapolate the shape of the object. Normally, the point clouds produced by (3D) scanners will not be used directly. Mostly all the applications using polygonal (3D) models, (NURBS) surface models, or ediTable feature-based (CAD) models. The process of converting a point cloud into a (3D) model in any forms described above is called 'reconstruction or "modeling"'.

Therefore, the reconstruction and modification is performed by utilizing CATIA software to creat (NURBS) surface model from point cloud and scale down as 65% in order to fit with small experimental machine. After having (CAD) model, we proposed two methods to obtain (CL) data and simulation process as shown in Figure 4.4.

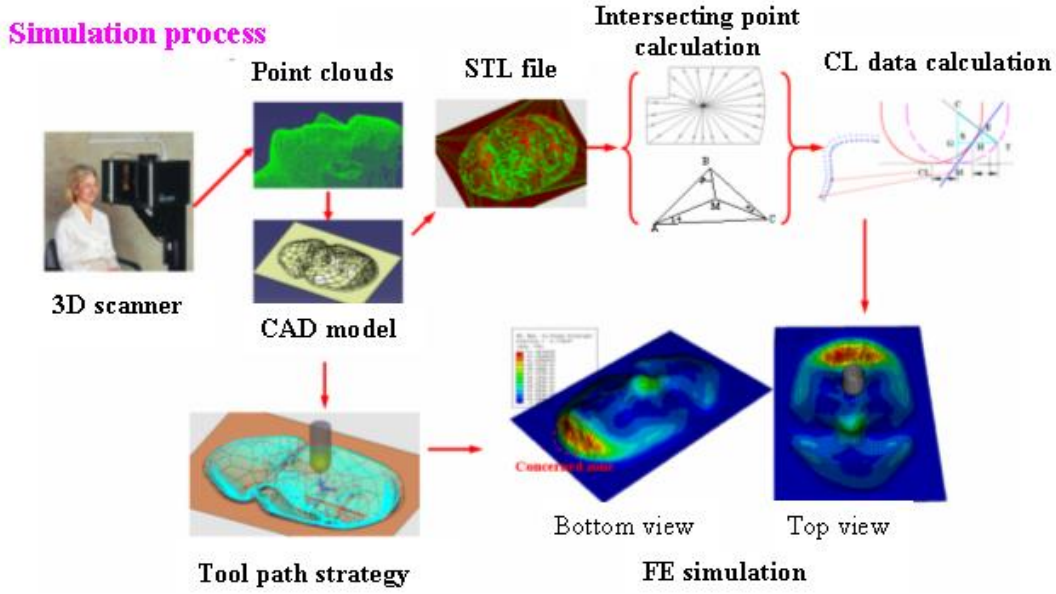

Figure 4.4: *The method to obtain CL data and simulation process.*

The first method is a basic programming method by using MALAB software. Following this method, initially the (CAD) model was saved to STL (standard triangulation language) file which consists of an unordered list of triangular facets representing the outside surface of the object. These triangular facets are described by a set of *X*, *Y* and *Z* co-ordinates for each of the three vertices and a unit normal vector with *X*, *Y* and *Z*. In order to generate inside intersection points of triangular which will be used to calculate cutter location (CL) at each Z layer of tool down-step, we first projected *n* divisions following radial direction from center axis and calculated intersection points of projection line and the planes containing three vertices of triangular. The intersection points must be then verified whether the points are insides or outsides of triangular as shown in Figure 4.5 in order to get all insides.

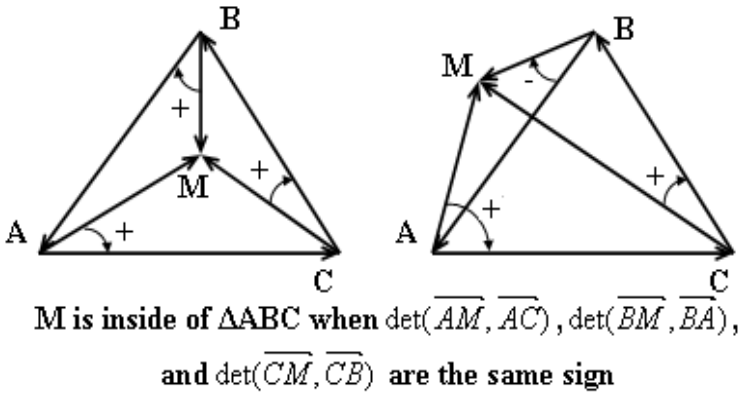

Figure 4.5: *Verification of the intersection points.*

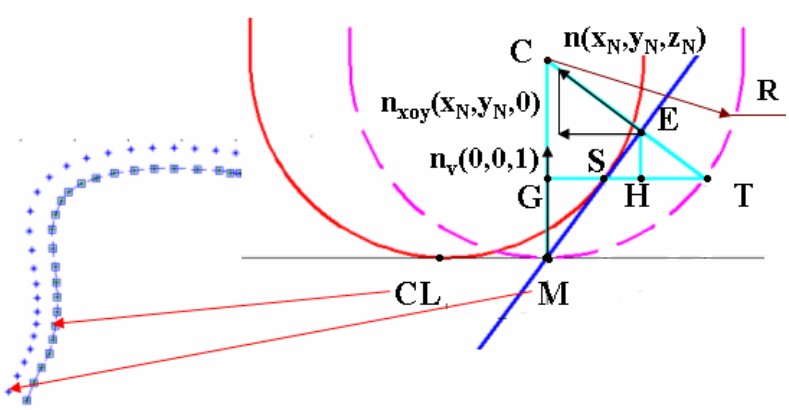

Figure 4.6: *Calculation of cutter location (CL) points.*

Finally, as depicted in Figure 4.6 from inside intersection points we can calculate (CL) points following listed Equations:

$$c = m + Rn_v$$

$$t = c - Rn_n$$

$$|CE| = |CG| = |Rn_v n_n|$$

$$e = c - |CE|n_n$$

$$|ET| = |E - T|$$

$$h = e - |ET|n_v$$

$$|ST| = \frac{(|ET|)^2}{|HT|}$$

$$cl = m + |ST|n_{xoy} \tag{4.1}$$

where *c, m, t, e, h, cl* are vectors corresponding to the tip points *C, M, T, E, H, CL*; R is tool radius; n_n is unit normal vector of triangular; n_v is unit vertical vector; n_{xoy} is the projective vector of n_n into xoy plane.

We also proposed a second method to obtain (CL) data from utilizing (CAM) software. Here, the (CAD) model was saved to (IGES) file and import to (CAM) software, namely CIMATRON E 6.0, that are used to generate (CL) data and also define the motion of the machines during processing. In this software, a Z-level milling operation is selected with spiral

tool path strategy and out-in downward movement of the tool (Figure 4.7). After simulation, the (CL) file, which includes the position of tool center point followed linear and circular interpolation, is generated and used to modify (CAE) input file.

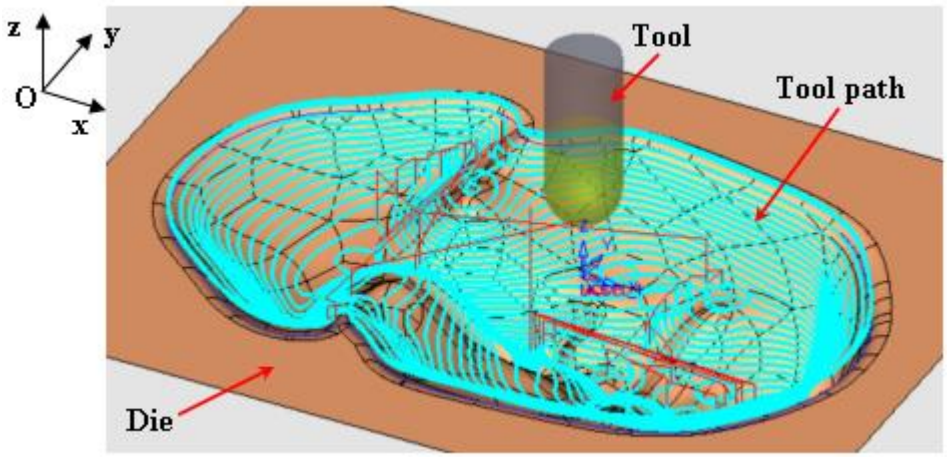

Figure 4.7: *Tool path strategy.*

4.3.2 CAE input file modifications

As mention in the second method, (CL) file includes linear and circular interpolations of the position of tool center point. Linear interpolations are easy to assign the forming tool movement in ABAQUS. But in circular interpolations, tool center point must be rotated around the other center points generated by (CAM) sofware, and it seems impossible to assign the forming tool movement in ABAQUS. So that in this study, a procedure has been completed, which scans the circular interpolations and divides them into linear segments satisfying allowable error.

By using ABAQUS, the forming tool movements are defined through the step module. It means that the movements are correlative with the steps of step module. Fortunately, there are more than thousand steps needed to simulate in incremental sheet forming process. If we operate the position of tool center point manually, it will take a lot of time and may be a chance of getting some manual error. So in this study, MATLAB software has been used as a programming tool to modify the (CL) data and also (CAE) input file.

Because the procedures for other steps are similar except values of position coordinates of tool center point. So firstly, the (CAE) input file is exported to get initial (CAE) input file. Then the text file of (CL) data is modified to obtain all position coordinate of tool center point as a standard (CL) data file through a subroutine of MALAB. Finally, in order to obtain final (CAE) input file, another MATLAB's subroutine had been written to add all next steps and assign values of tool center point from the standard (CL) data file to initial (CAE) input file for the correlative steps

4.4 Taguchi's Orthogonal Array

As above mentioned, many process variables contribute to enhancing the formability of incremental sheet forming process. If process variables are not suitably selected, a failure will appear at the concerned area. In this study, tool radius (*R*), tool down step (*H*), and the friction coefficient (μ) are considered as main process variables which govern the formability of material in incremental sheet forming. Thus, we try to verify and improve their influences on formability. For this kind of process, the failure was subjected to serious strain during the incremental sheet forming and found to be prone to internal or superficial micro-defects due to excessive tensile stress This initial damage and its growth then cause quality problems, such as necking and fractures, due to ductile tearing of the sheet. The reasons are that the high tensile stress and equivalent plastic strain at this area are larger than those in the other zones of the blank or the small difference between the major strains (ε_1) and the (FLC) values at the same point for the minor strains (ε_2) at the concerned area, (Figure 4.8)$(\Delta\varepsilon = \varepsilon_{FLC} - \varepsilon_1)$. The forming limit curve (FLC) in incremental sheet forming will be estimated and explained in more detail in Section 5. When changing the process variables, it was found that the magnitude of the difference in the major strain $(\Delta\varepsilon)$ and the integral value *I* also changed. Thus, it was concluded that the forming conditions of the product in incremental sheet forming could be improved.

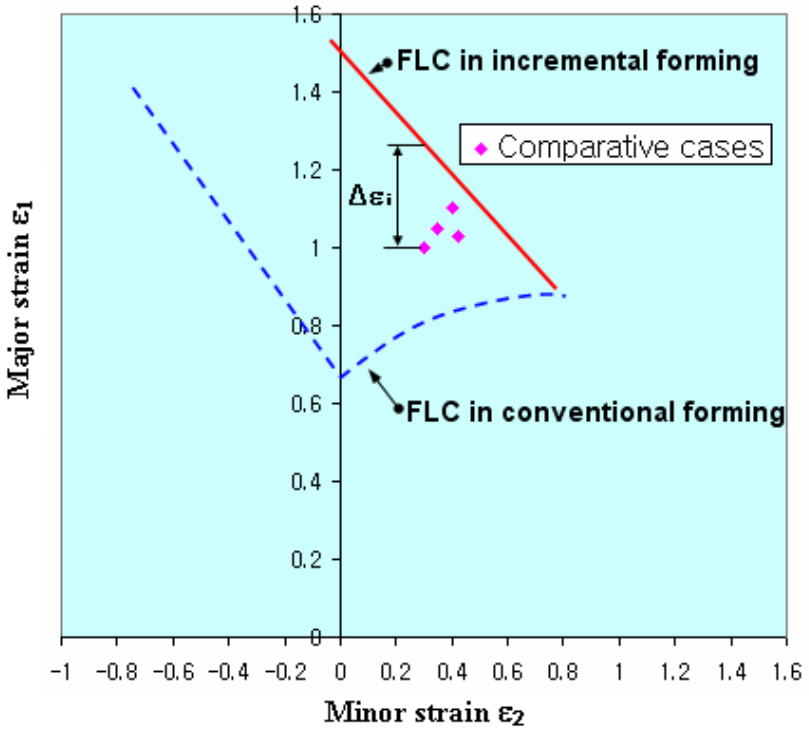

Figure 4.8: *Definition of the difference of major strain (Δε).*

In the preliminary study, the difference in the major strain$(\Delta\varepsilon)$ and the integral value *I* were set as the objective functions of the incremental sheet forming process. An analysis of the selected objective characteristics and values of the difference in the major strain$(\Delta\varepsilon)$ and the integral value *I* allowed the level of deviation to be calculated to identify which process variables were significant for the experiment.

When using this quality characteristic, the problem becomes a larger-the-better type problem in the case of the difference in the major strain$(\Delta\varepsilon)$ and smaller-the-better type problem in the case of ductile fracture criterion. Thus, according to the Taguchi method, the larger the difference in the major strain$(\Delta\varepsilon)$ and the smaller the integral value *I*, the better the incremental sheet forming process.

The signal-to-noise ratio (*S*/*N* ratio) defined according to the Taguchi method is:

$$\eta_i^1 = -10\, log_{10}(\Delta\varepsilon^{-2}) \tag{4.2a}$$

$$\eta_i^2 = -10\, log_{10}(I^2) \tag{4.2b}$$

Where η denotes the observed value (unit: dB). Since the maximizing procedure for the S/N ratio minimizes the press formability, the best conditions for the incremental sheet forming process can be obtained by maximizing (η_i)

Figure 4.9 presents the definition of the three defined process variables, while their selected levels are listed in Table 4.2.

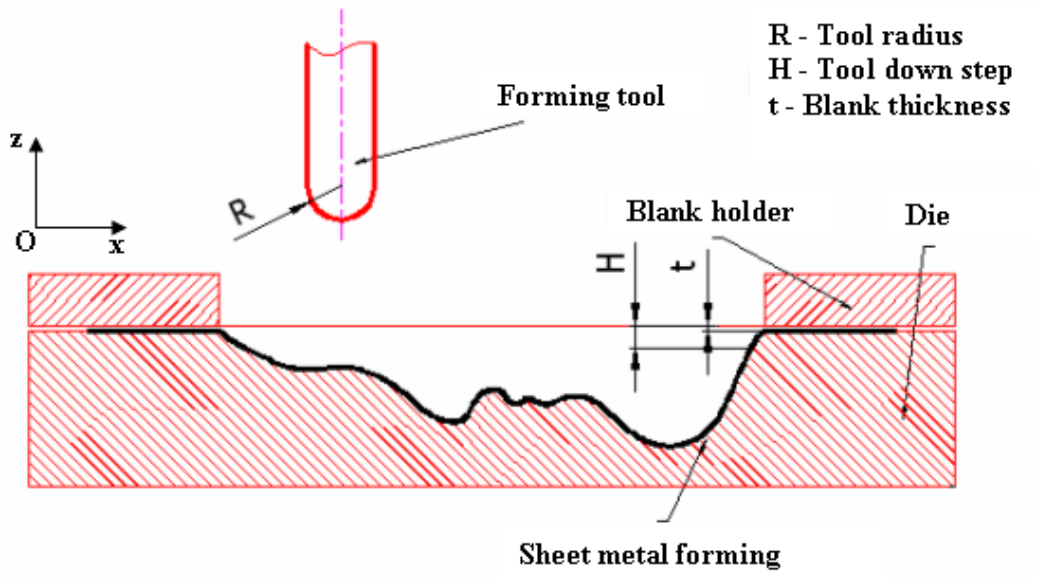

Figure 4.9: *Definition of considering parameters.*

Table 4.2: *Factors and their levels in FEM simulation*

Factors	Level		
	1	2	3
A (*R* mm)	6	5	4
B (*H* mm)	1.4	1.0	0.7
C (μ)	0.20	0.15	0.10
D (*t* mm)	1.0	1.0	1.0

As the FE simulation using the three factors with three levels gave nine degrees of freedom, a minimum of nine tests were required to investigate the effect on the FE simulation. Table 4.3 shows the L_9 orthogonal array chosen from Taguchi's standard-orthogonal-array Table. The number for each column is related to the level number for each factor. In this study, only the individual effects of each factor on the (FE) simulation were investigated, without considering the interactions between each factor.

Table 4.3: *Taguchi's L9 orthogonal array for simulations*

Case	A (*R* mm)	B (*H* mm)	C (μ)	D (*t* mm)
1	1(6)	1(1.4)	1(0.20)	1(1.0)
2	1(6)	2(1.0)	2(0.15)	1(1.0)
3	1(6)	3(0.7)	3(0.10)	1(1.0)
4	2(5)	1(1.4)	2(0.15)	1(1.0)
5	2(5)	2(1.0)	3(0.10)	1(1.0)
6	2(5)	3(0.7)	1(0.20)	1(1.5)
7	3(4)	1(1.4)	3(0.10)	1(1.0)
8	3(4)	2(1.0)	1(0.20)	1(1.0)
9	3(4)	3(0.7)	2(0.15)	1(1.0)

4.5 Estimation of FLC in incremental SHEET forming

To estimate the forming limit curve of the sheet, some conclusions from the previous researchers have been mentioned as follows:

- Swift's diffused necking criterion [51] for thin sheets and Hill's localized necking criterion [79] associated with the Hill's quadratic yield function [80] are used to construct the (FLC) in conventional forming (FLC at necking: FLCN) for the bi-axial tensile strain zone and tensile–compressive strain zone, respectively. So by using power law Equation (3.1), forming limit curve can be derived based on in-plane test (M-K model).

- From the previous literature [59, 77], most forming limit curves in incremental sheet forming (FLC at fracture: FLCF) appears to be a straight line with a negative slope in the positive region of the minor strain.

However, as a pointed out by several authors [81, 82] both of (FLCN) and (FLCF) curves at equi-biaxial strain nearly converge at one point. Thus, in the present study, the criterion of Clift et al [83] is employed in Equation (4.3) in order to calculate others points of (FLCF) in incremental sheet forming through the relationship of major/minor strain Equation (4.4), and the equivalent strain function for plane stress Equation (4.5) .

$$\int_0^{\bar{\varepsilon}_f} \bar{\sigma}\, d\bar{\varepsilon} = C \tag{4.3}$$

$$\beta = \frac{\varepsilon_2}{\varepsilon_1} \tag{4.4}$$

$$\bar{\varepsilon} = \frac{R_m+1}{\sqrt{2R_m+1}} \sqrt{1 + \frac{2R_m}{R_m+1}\beta + \beta^2}\,\varepsilon_1 \tag{4.5}$$

where $\bar{\varepsilon}_f$ is the equivalent strain at which the fracture occurs, $\bar{\sigma}$ is the equivalent stress, $\bar{\varepsilon}$ is the equivalent strain, C is the material constant, β is strain ratio, R_m is Lankford value, and ε_1, ε_2 are minor and major strains respectively.

After substituting power law Equation (3.1) into ductile fracture criterion Equation (4.3) and executing integral calculus we can derive the equivalent strain at the ductile fracture as a constant value Equation (4.6)

$$\bar{\varepsilon}_f = C_1 \tag{4.6}$$

To determine C_1 the values of strain ratio and major strain at equi-biaxial are used. The prediction of forming limits with the characteristic factors affecting the shape and level of the forming limits were implemented utilizing the algorithm developed by Son and Kim [84]. At equi-biaxial, the strain ratio β is 1.0, and the fracture major strains for the cases of tool radius R = 6 mm, R = 5 mm, and R = 4 mm was 0.98, 1.03 and 1.12, respectively. From this result, the constant values C_1 for the case of radius tool R = 6 mm, R = 5 mm and R = 4 mm were calculated as 2.27, 2.39 and 2.59, respectively. Finally, as depict in Figure 4.10, other points of (FLC) in incremental sheet forming were obtained by using various values of strain ratios and substituting into Equations (4.4), (4.5), and (4.6).

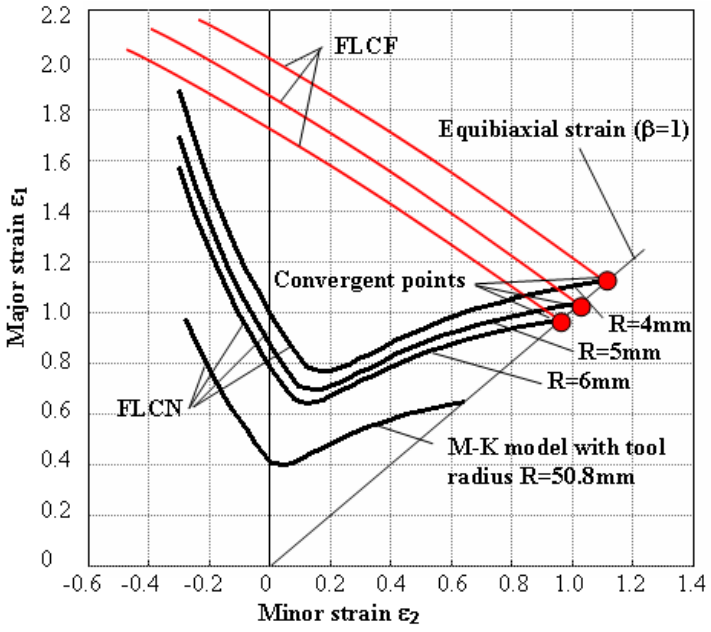

Figure 4.10: *Obtainment of FLC in incremental forming.*

4.6 Results and Discussion

In order to determine the scalar parameter β, the tensile curves, obtained by FE simulation via VUMAT user material through changing the values of β, was compared with the stress -strain experiment data which obtained from uniaxial tension test and then chosen the best fit. The scalar parameter β for isotropic/kinematic hardening was chosen as 0.65 as showed in Figure 4.11.

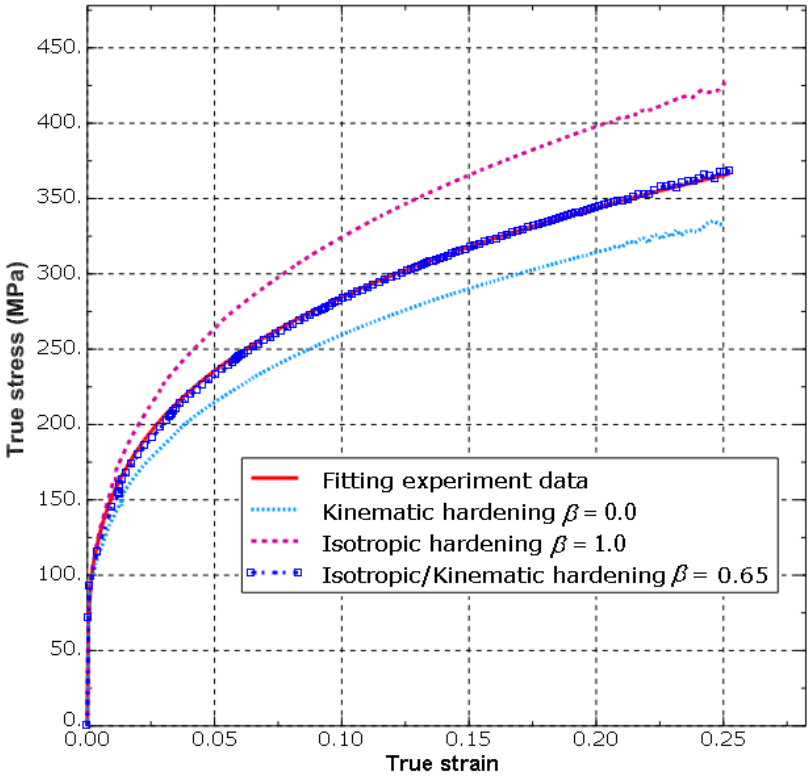

Figure 4.11: *Estimation of scalar parameter (β).*

Table 4.4 shows the results of the difference in the major strain$(\Delta\varepsilon)$ and the integral values I in numerical simulations based on a combined isotropic/kinematic hardening law for each case chosen from Taguchi's standard-orthogonal-array Table. The maximum value of the integral values *I* and minimum value of the difference in the major strain$(\Delta\varepsilon)$, i.e. the potential initial fracture site, appeared at the corner with large depth and slope angle value of the product for all cases. As mentioned before, the condition of failure was satisfied when and where the ductile fracture values *I* approached 1.0. For case no.2 and no.3, the ductile fracture values *I* were larger than 1.0, and failure appeared. The trends of the failure site predicted in this study were in good agreement with those in the actual product.

Table 4.4: *L_9 orthogonal array and calculated observed values*

Case	Column number and factor assignment			Ductile fracture value (I)		Difference in major strain ($\Delta\varepsilon$)	
	A (R mm)	B (H mm)	C (μ)	I	η_i^a (dB)	$\Delta\varepsilon$	η_i^b (dB)
1	1(6)	1(1.4)	1(0.20)	1.285	-2.178	-0.025	-32.041
2	1(6)	2(1.0)	2(0.15)	1.156	-1.259	0.115	-18.786
3	1(6)	3(0.7)	3(0.10)	1.054	-0.457	0.231	-12.729
4	2(5)	1(1.4)	2(0.15)	1.201	-1.591	0.061	-24.293
5	2(5)	2(1.0)	3(0.10)	1.078	-0.652	0.179	-14.943
6	2(5)	3(0.7)	1(0.20)	0.982	0.158	0.302	-10.400
7	3(4)	1(1.4)	3(0.10)	1.067	-0.563	0.197	-14.111
8	3(4)	2(1.0)	1(0.20)	1.031	-0.265	0.275	-11.213
9	3(4)	3(0.7)	2(0.15)	0.934	0.593	0.363	-8.802

According to the Taguchi method, an analysis of the mean (ANOM) and analysis of variance (ANOVA) were used to represent the relationship between the geometry factors for the concerned area and the observed values for the difference in the major strain$(\Delta\varepsilon)$ and ductile fracture value *I*. In this experiment, the observed values were found to be related to the three process variables (Table 4.4). The improvement of the observed values was then determined through a comparison with the Taguchi signal-to-noise (S/N) ratio. The (ANOVA) values calculated for the three factors and their corresponding three levels (tabulated in Table 4.2) were obtained using an L_9 orthogonal array. The use of orthogonal array reduced the full factorial design down to 9 experiments from 81 experiments, thereby decreasing the cost, time, and effort. The increase in the factor effect was measured using the S/N ratio of the factors. Moreover, the analysis of the mean (ANOM) and analysis of variance (ANOVA) for the quality characteristics provided a better understanding of the individual effect of each factor. The (ANOVA) for the different factors - including the level average, total variation, sum of the squares, sum of the mean squares, and contribution - enabled various relative quality effects to be determined. Table 4.5 shows a summary of the calculated results.

Table 4.5: *ANOM and ANOVA Table for effect of difference in major strain*$(\Delta\varepsilon)$

Factor	Average η by Level			Sum of Squares	D.O.F	Sum of mean squares	Contribution
	1	2	3				
A(R)	-21.185	-16.545	-11.375*	144.486	2	72.243	0.338
B(H)	-23.482	-14.981	-10.643*	255.911	2	127.9555	0.598
C(μ)	-17.885	-17.294	-13.927*	27.347**	2	13.6735	0.064
Total				427.744	6	213.872	
* Indicates the optimum level ** Indicates the sum of squares added to estimate the pooled error sum of squares in parentheses							

The formulation used to calculate the sum of the squares was as follows:

$$3(m_{j1} - m)^2 + 3(m_{j2} - m)^2 + 3(m_{j3} - m)^2 \quad (4.7)$$

Where m is the overall mean of the η_i, value for the nine experiments, defined as $m_1 = 1/9\sum_{i=1}^{9}\eta_i^2 = -16.369, m_2 = 1/9\sum_{i=1}^{9}\eta_i^2 = -0.691$ and m_{ji} is the average of η related to level i (i=1, 2, 3) of factor j given by $m_{ji} = 1/3\sum_{i=1}^{3}(\eta_j)_i$.

The results of the ANOM and ANOVA for the difference in the major strain$(\Delta\varepsilon)$ and ductile fracture value I (Table 4.5 and 4.6) revealed that the tool down-step (H), which reached 59.83% (Table 4.5) (60.72% (Table 4.6)), made the major contribution to the overall performance. Meanwhile, the contribution percentages for the tool radius (R) and friction coefficient (μ) were lower at 33.78% (Table 4.5) (37.92% (Table 4.6)) and 6.39% (Table 4.5) (1.69% (Table 4.6)), respectively. The contribution percentage of the friction coefficient (μ) was the smallest. Thus, it was concluded that the tool down-step (H) factor had the most significant effect on the press formability in the area of concern, while the effect of the friction coefficient (μ) was negligible.

Table 4.6: *ANOM and ANOVA Table of effect on ductile fracture value (I).*

Factor	Average η by Level			Sum of Squares	D.O.F	Sum of mean squares	Contribution
	1	2	3				
A(R)	-1.298	-0.695	-0.078*	2.231	2	1.1155	0.3792
B(H)	-1.444	-0.726	0.098*	3.573	2	1.7865	0.6072
C(t)	-0.762	-0.752	-0.557*	0.080	2	0.0400	0.0136
Total				5.884	6	2.942	
* Indicates optimum level ** Indicates sum of squares added to estimate pooled error sum of squares in parentheses							

The η (dB) of the levels for each factor were individually calculated, as shown in Table 4.4. In the Taguchi method, the higher the η value, the better the overall performance, meaning that the factor levels with the highest η value should always be selected. Accordingly, the average for each experimental level was calculated using the highest η value for each factor to produce the response Table (Tables 4.5 and 4.6). As shown in the response Table, the optimum conditions to maintain the difference in the major strain$(\Delta\varepsilon)$ and the ductile fracture value I successfully in the forming test were $A_3B_3C_3$, which means R = 4 mm, H = 0.7 mm, and μ = 0.10 mm.

Figure 4.12 depicts the evolution of (FE) simulation results for the optimum conditions (A_3B_3-C_3) in incremental sheet forming process. Figure 4.13 shows the experimental result for optimum case, where no failure appeared in the concerned area.

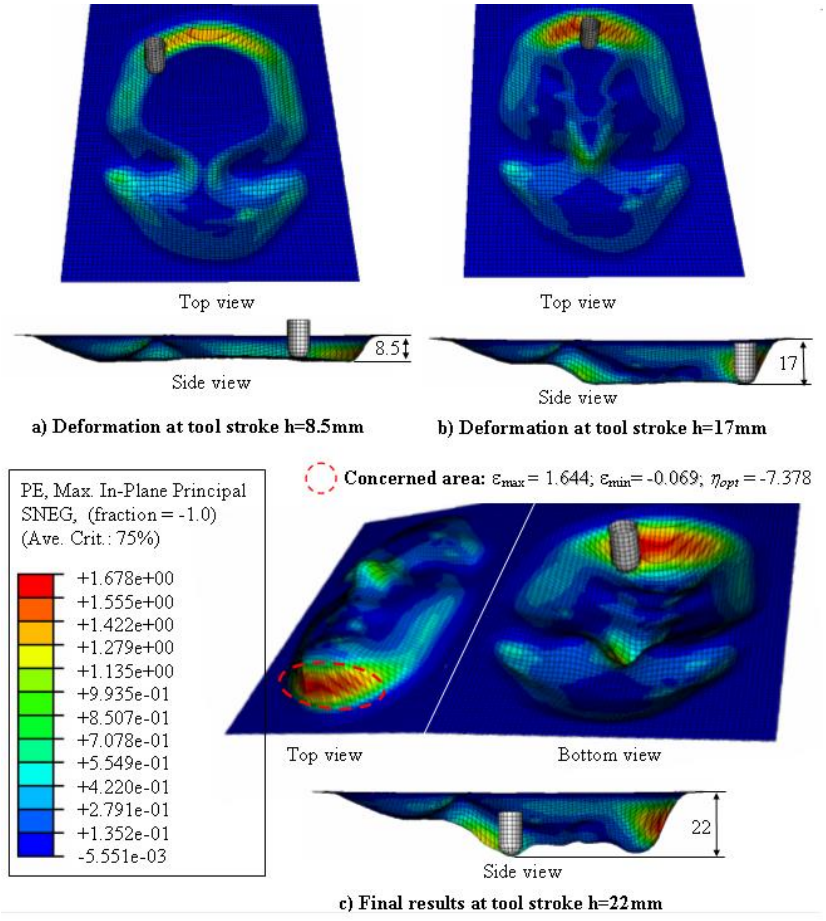

(i)

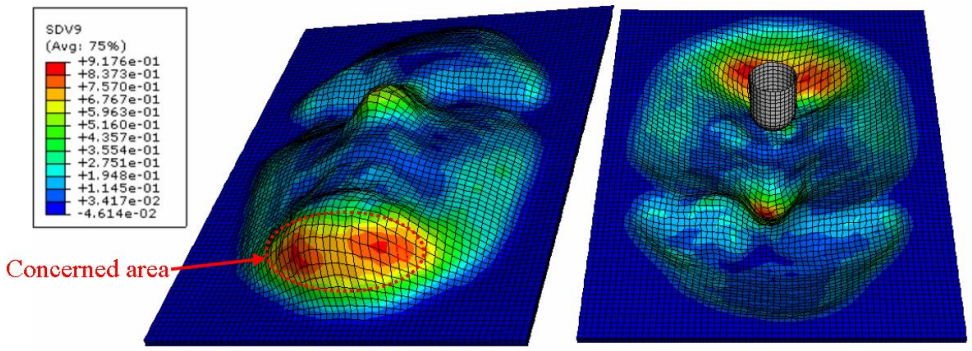

(ii)

Figure 4.12: *The evolution of deformed shape in FEM for optimum case of $A_3B_3C_3$ (i) and simulation result of I value (ii).*

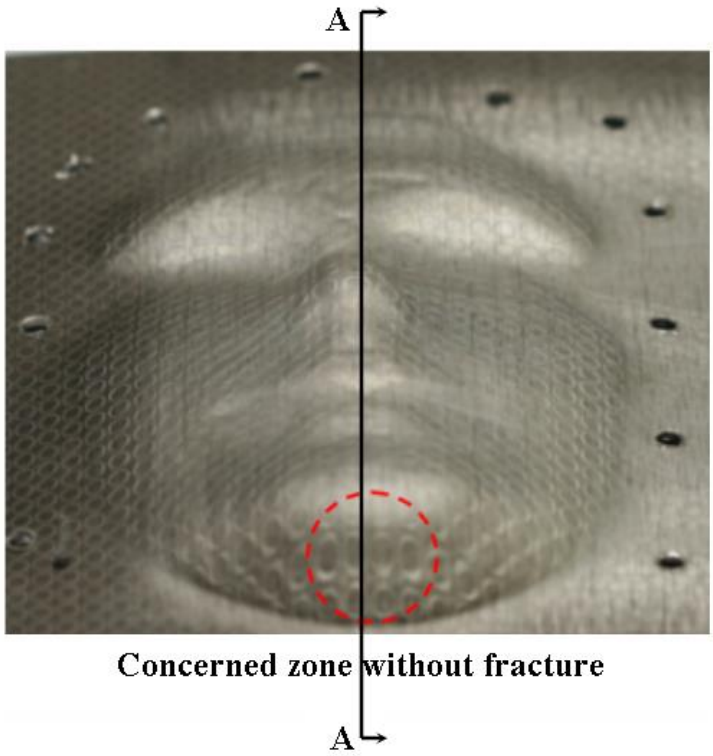

Figure 4.13: *Experimental result for optimum case of $A_3B_3C_3D_1$ (R=4mm, H=0.7mm, and $\mu=\mu_1=\mu_2=0.1$).*

Figure 4.14 presents the comparisons between cross-section views of evolutional stages of (FE) simulation and design section corresponding to side view in Figure 4.12 at each stage of tool stroke h = 8.5 mm, 17 mm, and 22 mm, respectively. Four different typologies of error can be detected on (FE) simulation results. First of all, a "pillow" effect can be highlighted at intermediate stages, determining a concave curvature of the under-formed material. Secondly, uncorrect tool paths generated at high slopes of sidewall, giving the big gap between final and design shape. Thirdly, due to a tool radius is larger than radii of curvature of design shape, although such inaccuracy is normally solved through using a smaller tool. Finally when the punch action is relaxed, the blank "lifts up" and the final depth of the part is lower than the design value.

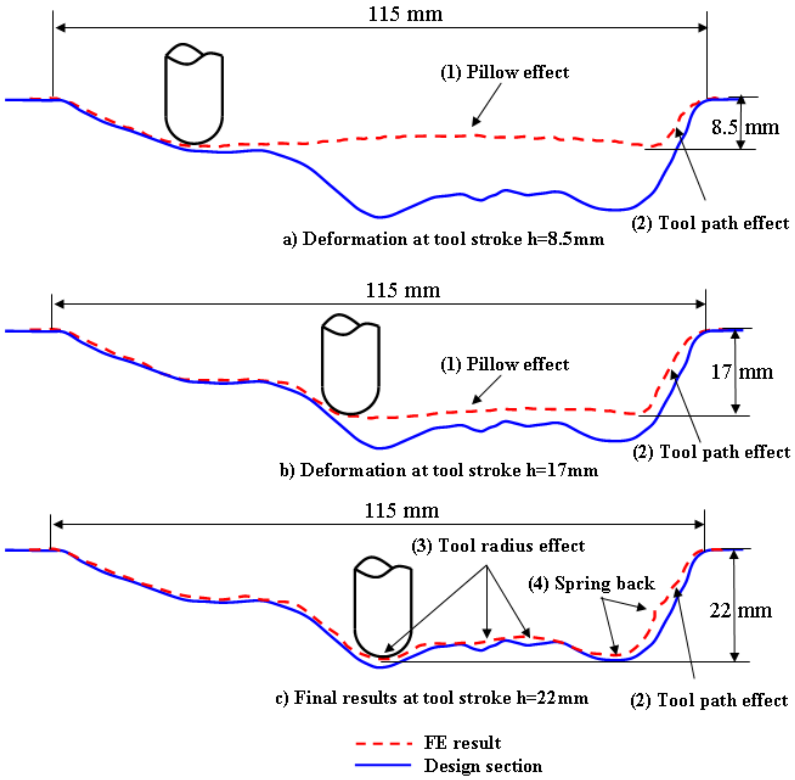

Figure 4.14: *Comparisons between section view of evolutional stages of FEM simulation and design section at tool stroke of h = 8.5mm, h = 17mm, and h = 22mm.*

To investigate and compare the accuracy of final shape between simulation and experiment, the cross-section AA in Figure 4.13 was measured to find out how much spring-back actually differed, see Figure 4.15. This figure shows that the difference of spring-back was larger at the surface profiles *cd* and *fg* due to the slopes of sidewall are larger than others surface profiles. The shape distribution of the surface profiles *ab*, *bc*, *de*, and *ef* has quite good agreement between the experimental and (FE) results.

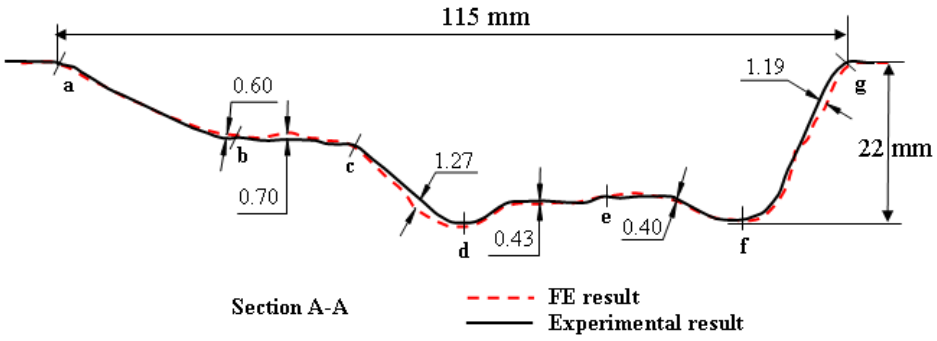

Figure 4.15: *Comparison of shape distribution between FE simulation and experiment results.*

From the above discussion, it was concluded that the use of Taguchi's experimental array for (FE) simulations allowed successful improvement of the process variables to improve the formability for incremental sheet forming process. As a result, the process variables were improved using a tool radius (R) of 4 mm, tool down step (H) of 0.7 mm, and friction coefficient (μ) of 0.1 mm.

4.7 Conclusion

To simulate the incremental sheet forming process of complex geometry shape e.g human face, values of (CL) data, which was generated from (CAM) simulation, has been automatically added and assigned to the (CAE) input file through MATLAB's subroutine programming.
To verify and improve process variables of incremental sheet forming process by using the finite element simulations, the tool radius, tool down step, and friction coefficient process variables was selected as main process variables and then investigated by the experiments. Commercial software (ABAQUS version 6.5, explicit formulation) was used for the simulation according to the orthogonal array of Taguchi's method. As a result of the (FE) simulations based on the Taguchi orthogonal array, the tool down step (H) was identified as the important factors for improving the formability of the incremental sheet forming process. An improved parameter, consisting of a tool radius (R) of 4 mm, a tool down step (H) of 0.7 mm, and friction coefficient (μ) of 0.1 mm, were chosen to give the best results for proposed geometry, using incremental forming.